Arch. Mech., 41, 5, pp. 735–746, Warszawa 1989

# Numerical prediction of turbulent flow in centrifugal compressor stage

K. P. SELEZNEV, Y. I. BIBA, B. N. SAVIN
and A. M. SIMONOV (LENINGRAD)

THE CALCULATION procedure of centrifugal compressor internal flow and losses based on the quasi-three-dimensional turbulent model is considered. The procedure includes the prediction of hub-to-shroud and blade-to-blade flows with tip-clearance flow, surface curvature, rotation and secondary flows being taken into account. A comparison of calculated results with experimental data is presented. Satisfactory agreement of local and energy parameters is achieved.

Przedstawiono procedurę obliczeniową do analizy wewnętrznych przepływów w sprężarce odśrodkowej, opartą na modelu quasi-trójwymiarowej turbulencji. Procedura ta obejmuje przepływy wewnętrzne i międzyłopatkowe uwzględniając przepływ przez szczelinę wierzchołkową, zakrzywienie powierzchni oraz przepływy wtórne. Obliczone wyniki porównano z danymi eksperymentalnymi. Stwierdzono dobrą zgodność parametrów lokalnych i globalnych (energii).

Представлена расчетная процедура для анализа внутренних течений в центробежном компрессоре, опирающаяся на модели квазитрехмерной турбулентности. Эта процедура охватывает внутренние и междулопастные течения, учитывая течение через верхнюю щель, искривление поверхности, а также вторичные течения. Вычисленные результаты сравнены с экспериментальными данными. Констатировано хорошее совпадение локальных и глобальных параметров (энергии).

## Nomenclature

$A$ Van-Driest damping factor,
$a$ sonic velocity,
$b$ meridional channel width,
$C$ absolute velocity,
$D$ impeller diameter,
$F$ mass force,
$H = 1-\sigma y$, $H_l = 1-\sigma n$ Lamé coefficients,
$h$ thickness of the layer between axisymmetric flow surfaces,
$i$ enthalpy,
$i^*$ stagnation enthalpy,
$L, L_0$ mixing lengths,
$\dot{M}$ source term modelling secondary flow,
$M_u = u_2/a$ symbolic Mach number,
$\overline{m}$ mass flow ratio,
$N$ external force capacity,
$n$ distance to the surface,
$n_w = W_1/W_2$ velocity ratio,
$p$ pressure,
$Q$ surface area,

| | |
|---|---|
| Ri | Richardson, number, |
| $r$ | radius, |
| $\omega r = u$ | velocity of surface rotation, |
| $V$ | volume, |
| $v_*$ | dynamic velocity, |
| $W$ | relative inviscid velocity, |
| $w$ | relative boundary layer velocity, |
| $(x, y, \varphi)$, $(l, n, z)$ | coordinates related to the surfaces, |
| $z_0$ | number of blades, |
| $\alpha$ | absolute flow angle, |
| $\beta$ | relative flow angle, |
| $\beta_c$ | empirical coefficient, |
| $\gamma$ | angle between axisymmetric flow surface and rotary axis, |
| $\delta$ | boundary layer thickness, |
| $\delta^*$, $\delta^{**}$, $\delta^{***}$ | integral boundary layer thicknesses, |
| $\delta_b$ | blade thickness, |
| $\Delta\psi$ | grid step, |
| $\Delta\varphi_s$ | angular separation region width, $\Delta s$ — tip-clearance width, |
| $\eta$ | efficiency coefficient, |
| $\zeta$ | loss coefficient, |
| $\nu$ | kinematic viscosity, |
| $\omega$ | angular velocity, |
| $\varrho$ | density, |
| $\sigma$ | surface curvature, |
| $\Phi = 4\bar{m}/(\pi\varrho_1 D_2^2 u_2)$ | flow rate coefficient, |
| $\Phi_0$ | flow rate coefficient at the optimal regime, |
| $\tau$ | shear stress, |
| $\tau_0$ | flow cluttering coefficient. |

**Subscripts**

| | |
|---|---|
| bb | blade-to-blade losses, |
| $e$ | effective viscosity, |
| fr | friction losses, |
| hs | hub-to-shroud losses, |
| imp | impeller losses, |
| $l, n, z$ | vector components of $(l, n, z)$ coordinate system, |
| $m$ | molecular viscosity, |
| mix | mixing losses, |
| pr | pressure side of the blade, |
| $s$ | separation point, |
| sec | secondary flow, |
| su | suction side of the blade, |
| $t$ | turbulent viscosity, |
| vd | vaneless diffusor losses, |
| $w$ | wall parameter, |
| $(x, y, u)$ | vector components of $(x, y, \varphi)$ coordinate system; |
| 1 | blade row inlet, |
| 2 | blade row outlet, |
| 3 | vaneless diffusor inlet, |

4 vaneless diffusor exit,
I hub surface,
II shroud surface.

## 1. Introduction

DESIGNING of effective centrifugal compressor stages with mixed-flow impellers is one of the main directions in turbomachinery. Wide spectrum of applications and high total energy consumption make a demand on centrifugal compressor efficiency. Now the numerical prediction of viscous flow can be successfully applied in designing centrifugal compressor internal flow channels.

The importance of internal flow channel designing based on aerodynamical analysis rises the experimental research cost. Numerical solution of the centrifugal compressor stage internal turbulent flow, representing a complex problem, is found by employing three-dimensional the Reynolds equations. The quasi-three-dimensional model [1] simplifies the spatial problem by dividing it into two two-dimensional ones.

## 2. Flow model

The model based on the quasi-three-dimensional formulation allows to calculate viscous flow parameters and stage losses. Some of the flow regions are considered as: 1) hub-to-shroud axisymmetrical viscous flow with introduced body forces replacing the blades flow influence; 2) blade-to-blade flow with inviscid core and turbulent boundary layer.

The axisymmetric streamline surface positions are determined by preliminary impeller hub-to-shroud inviscid flow calculations. The blade-to-blade flow is simulated by the assumption of existence. the inviscid core and turbulent boundary layer. Inviscid blade-to-blade and hub-to-shroud flows can be presented by one of the known methods [1, 2]. For pressure differences between the suction and pressure sides of the blade, the body force $F$ replacing the blades flow effect are determined on various axisymmetrical streamline surfaces and used in the following turbulent axisymmetric hub-to-shroud impeller flow calculations.

## 3. Hub-to-shroud flow

The curvilinear orthogonal coordinate system connected with the region geometry is used (Fig. 1). The values $y = -0.5$ and $y = 0.5$ correspond to the hub and shroud impeller surfaces, respectively.

Thin-layer equations of axisymmetric turbulent flow are

$$\frac{\partial}{\partial x}(\varrho rbC_x) + \frac{\partial}{\partial y}(\varrho rHC_y) = 0, \tag{3.1}$$

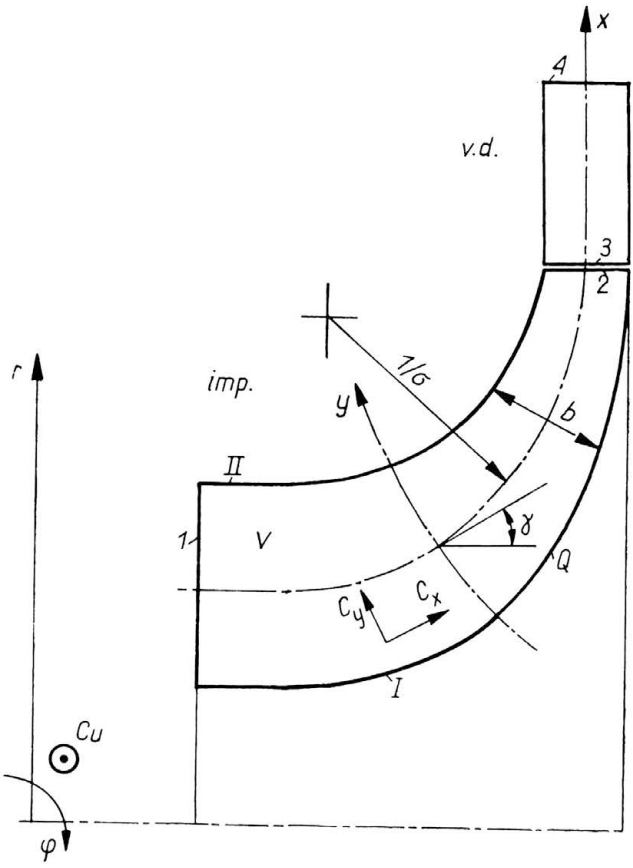


FIG. 1. Coordinate system for turbulent hub-to-shroud calculations in the impeller and vaneless diffusor.

$$(3.2)\quad \frac{C_x}{H}\frac{\partial C_x}{\partial x}+\frac{C_y}{H}\frac{\partial C_x}{\partial y}-\frac{\sigma C_x C_y}{H}-\frac{C_u^2}{rH}\sin\gamma = -\frac{1}{\varrho H}\frac{\partial p}{\partial x}+\frac{1}{b}\frac{\partial}{\partial y}\left[\nu_e\left(\frac{1}{b}\frac{\partial C_x}{\partial y}+\frac{\sigma C_x}{H}\right)\right]+\frac{1}{r}\nu_e\left(\frac{1}{b}\frac{\partial C_x}{\partial y}+\frac{\sigma C_x}{H}\right)-\frac{2\sigma}{Hb}\nu_e\frac{\partial C_x}{\partial y}+F_x,$$

$$(3.3)\quad \frac{\sigma C_x^2}{H}\frac{C_u^2}{rb}\cos\gamma = -\frac{1}{\varrho b}\frac{\partial p}{\partial y},$$

$$(3.4)\quad \frac{C_x}{H}\frac{\partial C_u}{\partial x}+\frac{C_y}{b}\frac{\partial C_u}{\partial y}+\frac{C_x C_p}{rH}\sin\gamma+\frac{C_y C_u}{r}\cos\gamma = \frac{1}{b}\frac{\partial}{\partial y}\left[\nu_e\left(\frac{1}{b}\frac{\partial C_u}{\partial y}-\frac{C_u}{r}\cos\gamma\right)\right]-\frac{\sigma}{Hb}\nu_e\frac{\partial C}{\partial y}+\frac{2}{r}\nu_e\left(\frac{1}{b}\frac{\partial C_u}{\partial y}-\frac{C_u}{r}\cos\gamma\right)\cos\gamma+F_u,$$

$$(3.5) \qquad b \int_{-0,5}^{0,5} \varrho r C_x dy = \text{const}(x),$$

where Eq. (3.1) is the continuity equation, Eqs. (3.2), (3.3), (3.4) are components of the momentum equation; Eq. (3.5) is the flow ratio equation. The turbulent viscosity can be written according to [3] as

$$(3.6) \qquad \nu_t = L^2 \sqrt{\left[\frac{H}{b}\frac{\partial}{\partial y}\left(\frac{C_x}{H^2}\right)\right]^2 + \left[\frac{r}{b}\frac{\partial}{\partial y}\left(\frac{C_u}{r}\right)\right]^2}.$$

The mixing length $L$ is determined by the two-layer model [4] with consideration of curvature according to the Monin–Obuchov formulae:

$$(3.7) \qquad L = L_0\,[1-\beta_c(\mathrm{Ri}_x+\mathrm{Ri}_u)], \qquad L_0 = \min\left\{0.4n;\ 0.09\,\frac{b}{2}\right\}, \qquad \beta_c = 6,$$

Richardson numbers are

$$(3.8) \qquad \mathrm{Ri}_x = \frac{2C_x\sigma b}{H\dfrac{\partial}{\partial y}\left(\dfrac{C_x}{H}\right)}, \qquad \mathrm{Ri}_u = \frac{2bC_u\cos\gamma}{r^2\dfrac{\partial}{\partial y}\left(\dfrac{C_u}{r}\right)}.$$

Zero boundary conditions along hub and shroud surfaces are

$$(3.9) \qquad C_x = 0, \quad C_y = 0, \quad C_u = 0 \quad \text{or} \quad C_u = U \quad \text{for} \quad y = \pm 0.5.$$

At the channel inlet profiles of $C_x(y)$, $C\,(y)$ and the pressure level are given.

Compressibility is considered approximately: density is assumed to vary in streamline direction only and it is determined from the gas state equation. The temperature is calculated by assuming that the heat transfer to the outer region vanishes. The approximate form of the stagnation enthalpy equation is

$$(3.10) \qquad i = i^* - \frac{\langle C^2\rangle}{2} + \frac{N}{\bar{m}},$$

where $\langle C^2\rangle$ is the averaged squared velocity. Body forces vector components are calculated as

$$(3.11) \qquad F_u = (W_{su}^2 - W_{pr}^2)/(4\pi r\tau_0), \qquad F_x = F_u \cdot \operatorname{ctg}\beta.$$

The numerical solution of the problem (3.1)–(3.11) is carried out by means of the implicit four-points finite-difference algorithm [5].

Zero boundary conditions are realized by using the wall-functions analogous to the logarithm velocity profiles [6] for curvilinear flows with proper pressure gradient and body forces.

The axisymmetric turbulent flow solution in the vaneless diffusor is the special case of the problem (3.1)–(3.11) solution for $\mathbf{F} = 0$, according to the flow model considered.

## 4. Blade-to-blade flow

The solution of turbulent boundary layer at the blade along the axisymmetric streamline surface is found by considering of surface curvature, secondary flows and the tip-clearance flow. The curvilinear orthogonal coordinate system is used (Fig. 2). Coordinate $l$ is parallel

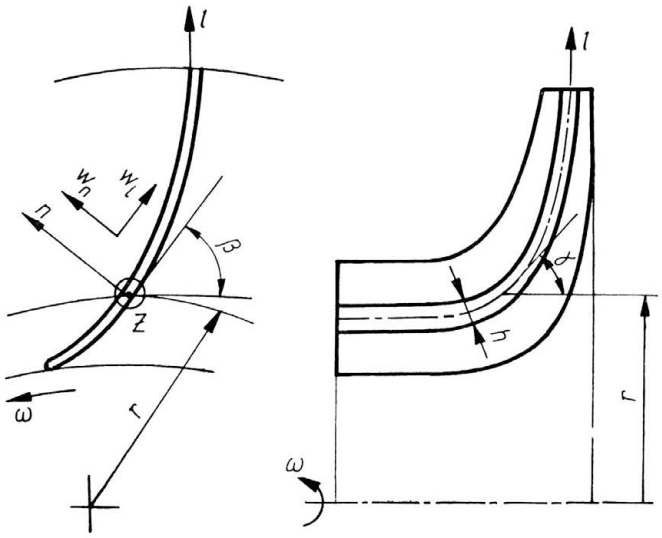


FIG. 2. Coordinate system for boundary layer calculations on the impeller blade surfaces along axisymmetric streamline surface.

to the blade surface, $n$ is perpendicular to it, surface $(l, n)$ is tangent to the axisymmetric streamline surface, $z$ is normal to it.

Equations of the turbulent boundary layer at the curvilinear surface (secondary flow being neglected) are

$$(4.1)\qquad w_l\frac{\partial w_l}{\partial l}+w_n H_l\frac{\partial w_l}{\partial n}+w_l w_n\sigma = W\frac{dW}{dl} - \frac{\partial}{\partial l}\int_n^{\delta}\left(\sigma\frac{w_l^2}{H_l}+2\omega w_l\sin\gamma\right)dn+\frac{H_l}{\varrho}\frac{\partial\tau}{\partial n}-2\tau\sigma+2H_l w_n\omega\sin\gamma,$$

$$(4.2)\qquad \frac{\partial}{\partial l}(\varrho w_l h)+\frac{\partial}{\partial n}(\varrho H_l h w_n)+\dot{M}=0,$$

where $\sigma$ is the curvature of the blade surface.

The shear stress is

$$(4.3)\qquad \tau=\varrho\nu_e\frac{\partial(w_l/H_l)}{\partial n}.$$

Turbulent viscosity, according to the Cebeci–Smith model [7], is equal to

$$\nu_t = L^2 H_l \frac{\partial}{\partial n}(w_l/H_l) \quad \text{(Prandtl formulae)} \tag{4.4}$$

in the wall region, and

$$\nu_t = 0.0168 W \delta^* \quad \text{(Clauser formulae)} \tag{4.5}$$

in the outer region.

The mixing length $L$ is calculated by considering the effects of curvature and rotational influence according to the Monin–Obuchov formulae:

$$L = L_0(1-\beta_c \mathrm{Ri}), \qquad \mathrm{Ri} = \frac{2\omega \sin\gamma - w_l \sigma}{H_l \dfrac{\partial}{\partial n}(w_l/H_l)},$$

$$L_0 = 0.4n\left[1-\exp\left(-v_* \frac{n}{A\nu_m}\right)\right], \qquad v^* = \sqrt{\tau/\varrho}, \tag{4.6}$$

$$A = 26\left(1-11.8\nu_m \frac{W}{v_*^3}\frac{dW}{dl}\right)^{-1/2}.$$

Equations (4.1) and (4.2) are solved under the following boundary conditions:

$$\begin{cases} w_l = 0, \quad w_n = w_{nw} & \text{by} \quad n = 0, \\ w_l = W_l & \text{by} \quad n = \delta, \end{cases} \tag{4.7}$$

where $W_l = (2\delta\omega\sin\gamma + W)/H_l$. The value $w_{nw}$ is calculated by analogy with the Couette solution of constant turbulent viscosity tip–clearance flow,

$$w_{nw} = \frac{\Delta s}{4h}\left[\omega r + \sqrt{(\omega r)^2 + \frac{W_{su}^2 - W_{pr}^2)\cdot \Delta s}{48 \cdot 0.0168 \delta_b}}\right]. \tag{4.8}$$

The source term $\dot{M}$ in the continuity equation characterizes the secondary flow influence by blowing (drain) of the fluid parallel to the surface and perpendicular to the streamline [8]. We assume that the secondary flow velocity profiles are similar to those at the blade and at the meridional surface. Then, using the relations obtained in [1], we have

$$w_{\mathrm{sec}} = \varepsilon W[1-(w_l/W)^3]\cdot(w_l/W), \tag{4.9}$$

where $\varepsilon = \mathrm{tg}\Delta\beta$, $\Delta\beta$ is the angle of limited streamline from the main flow on the meridional surface, and

$$\dot{M} = \frac{\partial(w_{\mathrm{sec}} H_l \varrho)}{\partial z}. \tag{4.10}$$

Substituting $w_l/W$ by "one seventh"-law, and averaging $\dot{M}$ over $y$ and $z$, we obtain

$$\dot{M} = 0.175 W[\mathrm{tg}(\Delta\beta)_{\mathrm{II}} - \mathrm{tg}(\Delta\beta)_{\mathrm{I}}]/b. \tag{4.11}$$

To achieve a good accuracy of the finite-difference solution of the equations (4.1)–(4.2), it is essential to concentrate the numerical grid points near the blade surface by means of a new coordinate system:

$$\xi = l, \quad \psi = \frac{n}{\delta(l)g(n)}, \tag{4.12}$$

where $g(n)$ is the function of point concentration. It reduces the grid step $\Delta\psi$ close to the blade surface according to the power-law

$$\Delta\psi_i = \Delta\psi_{\max}\left(\frac{\Delta\psi_{\min}}{\Delta\psi_{\max}}\right)^{\frac{i-1}{I}}, \tag{4.13}$$

I is the total number of grid intervals, $i$ is the number of the interval considered.

The numerical procedure of solving the problem (4.1)–(4.10) is carried out by a marching six-points finite-difference procedure [5] and by using nonuniform grid generation (4.12)

Integral boundary layer thicknesses are obtained in the form

$$\delta^* = \int_0^\delta \left(1 - \frac{w_l H_l - 2\omega \sin\gamma \cdot n}{W}\right) \frac{dn}{H_l}, \tag{4.14}$$

$$\delta^{**} = \int_0^\delta \frac{w_l H_l - 2\omega \sin\gamma \cdot n}{W} \left(1 - \frac{w_l H_l - 2\omega n \sin\gamma}{W}\right) \frac{dn}{H_l}, \tag{4.15}$$

$$\delta^{***} = \int_0^\delta \frac{w_l H_l - 2\omega n \sin\gamma}{W} \left[1 - \left(\frac{w_l H_l - 2\omega \sin\gamma \cdot n}{W}\right)^2\right] \frac{dn}{H_l}. \tag{4.16}$$

Mixing losses related to separation are essential in the general loss balance. Usually the separation region is developed at the suction side where the local flow breaking is strong. To make the separation point position more accurate, it is essential to consider the unbalanced boundary layer influences [7] in turbulence simulation, i.e., by changing the turbulent boundary layer structure up to separation. That is why the modified Clauser formula [9] is used.

## 5. Loss model

The internal stage flow energy losses are determined near the zero inlet flow angles as follows. According to the asumption, the impeller flow energy losses can be subdivided into blade losses calculated using the blade-to-blade solution, and surface losses calculated by means of the hub-to-shroud solution. Blade losses consist of friction blade losses and the mixing ones related to the exit flow separation near the suction side of the blade. These losses related to the secondary flows and tip-clearance flow, are usually included in the blade-to-blade boundary layer losses.

The efficiency of the stage is equal to

$$\eta = 1-\Delta\eta = 1-\Delta\eta_{\text{imp}}-\Delta\eta_{\text{vd}}, \tag{5.1}$$

where

$$\Delta\eta_{\text{imp}} = \Delta\eta_{\text{hs}}+\Delta\eta_{\text{bb}}.$$

The hub-to-shroud losses include the losses of hub and shroud surfaces, the losses of turbulent flow core and the losses connected with the hub-to-shroud secondary flows,

$$\Delta\eta_{\text{hs}} = 1-\frac{\int\limits_V \mathbf{C}\cdot\nabla p\,dV+\int\limits_2 \varrho\frac{C^2}{2}C_x dQ-\int\limits_1 \varrho\frac{C^2}{2}C_x dQ}{\int\limits_V \varrho\mathbf{C}\cdot\mathbf{F}\,dV+\int\limits_{II}\tau_{uy}C_u dQ-\int\limits_I \tau_{uy}C_u dQ}. \tag{5.2}$$

Blade-to-blade losses are determined from the boundary layer thicknesses both on the suction and pressure sides of the blade,

$$\Delta\eta_{\text{bb}} = \zeta_{\text{bb}}\frac{W}{2(C_{u2}U_2-C_{u1}U_1)}, \tag{5.3}$$

where

$$\zeta_{\text{bb}} = \zeta_{\text{mix}}+\zeta_{\text{fr}},$$

$$\zeta_{\text{fr}} = \left(\frac{W_2}{W_1}\right)^2 \sin^2\beta_2\,\overline{\delta^{***}}/(\sin\beta_2-\overline{\delta^*})^3,$$

$$\zeta_{\text{bb}} = \left(\frac{W^2}{W_1}\right)^2 \sin^2\beta_2\,\frac{2\overline{\delta^*}\left(\frac{1}{\sin\beta_2}-1\right)+(\overline{\delta^*})^2\frac{2\sin\beta_2-1}{\sin^2\beta_2}}{(\sin\beta_2-\overline{\delta^*})^2}$$

with the following boundary layer thicknesses:

$$\overline{\delta^*} = (\delta_{b2}+\Delta\varphi_s\cdot 2\pi r\tau_{02}/z_0+\delta^*_{\text{pr}})/(2\pi r_2/z_0),$$

$$\overline{\delta^{**}} = [(\delta^{**}_{\text{su}}\varrho b)_s/(\varrho_2 b_2)+\delta^{**}_{\text{pr}}]/(2\pi r_2/z_0),$$

$$\overline{\delta^{***}} = [(\delta^{***}_{\text{su}}\varrho b)_s/(\varrho_2 b_2)+\delta^{***}_{\text{pr}}]/(2\pi r_2/z_0).$$

## 6. Numerical results

As shown in Fig. 3, there is satisfactory agreement of the static pressure values achieved. The discrepancy is observed at high negative inlet flow angles, when the local separation region is formed near the blade and the flow cluttering suddenly increases what leads to an increase of velocity. The cause of the existence of a low pressure region at the impeller inlet has not been established in calculations.

Thus the results presented show the possibility of approximate estimation of real flow parameters by means of the regimes close to the optimum ones.

Boundary layer velocity profiles show (Fig. 4) the growth of boundary layer thickness from blade row inlet to outlet, and the effect of the blade surface curvature on the profile.

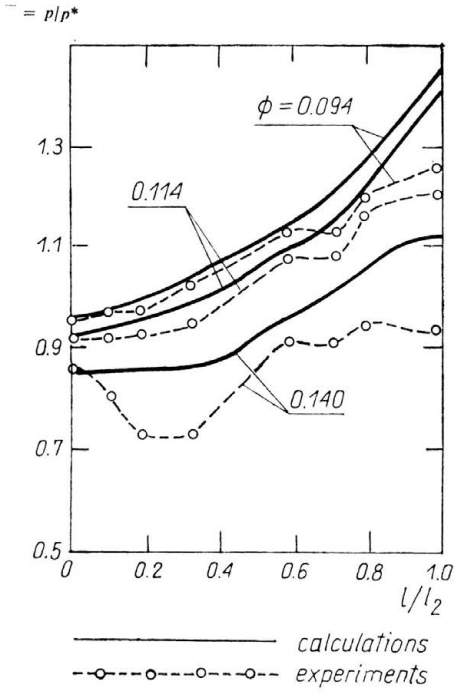


FIG. 3. Static pressure distributions along shroud surface of the mixed-flow impeller for various flow rate coefficients. Dimensionless inlet shroud diameter $\bar{D}_{s1} = 0.61$, relative exit blade height $b_2 = b_2/D_2 = 0.04$.

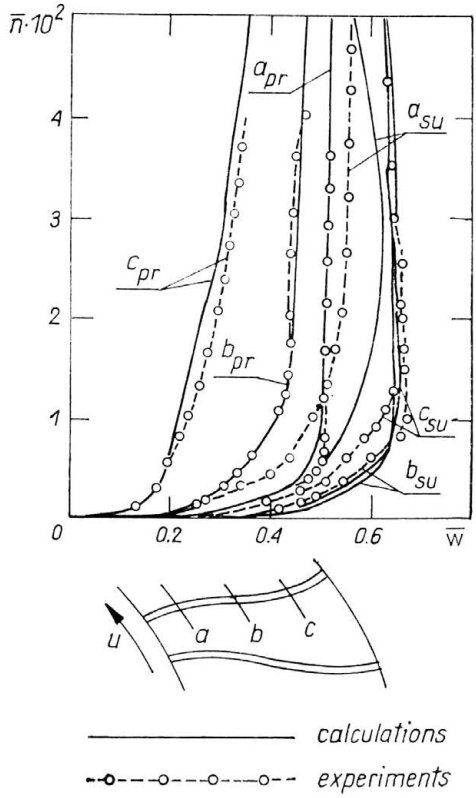


FIG. 4. Boundary layer velocity profiles along the middle streamline blade surface, $\Phi = 0.065$, $\bar{n} = nz_0/(2\pi r_2)$, $w = w/u_2$.

Figure 5 shows the calculated and experimental efficiencies of impellers and stages with vaneless diffusors having different values of impeller velocity ratio $n_w$. Stages for different flow rate coefficients $\Phi_0 = 0.04...0.09$ were investigated for

$$M_u = 0.78, \quad \bar{b}_3 = \frac{b_3}{b_2} = 1.0, \quad \bar{D}_4 = \frac{D_4}{D_2} = 1.8.$$

It is shown that the impeller and stage efficiencies calculated have maxima depending on $n_w$ and $\Phi_0$. Maximum efficiency values decreases with decreasing $\Phi_0$. Optimal values of $n_w$ lie between $n_{w\text{opt}} = 1.2$ and 1.3. In the interval $n_w < n_{w\text{opt}}$ decreasing of $\eta$ is related to the increase of the relative height of the channel. In the interval $n_w > n_{w\text{opt}}$ the efficiency increases with increasing $n_w$ as a result of growing breaking losses. They are intensified with ncreasing velocity ratio. No maxima were established at the experimentally determined va lues of the efficiency as a function of the velocity ratio. They probably lie in the region

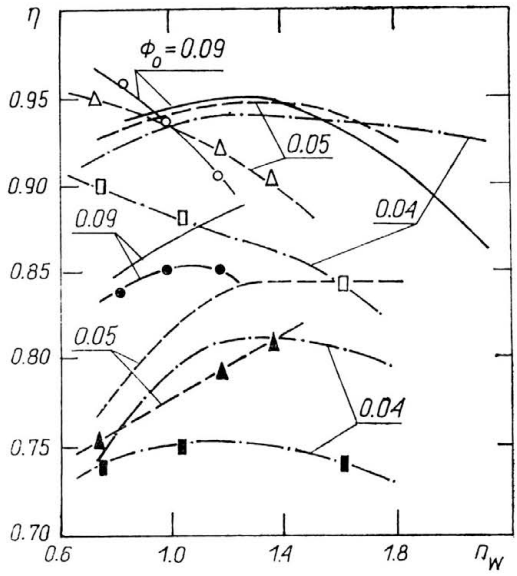


| $\Phi_0$ | experiments | | calculations |
|---|---|---|---|
| | imp | stage | |
| 0.09 | —●— | —○— | ——— |
| 0.05 | —▲— | —△— | – – – – |
| 0.04 | —■— | —□— | —·—·— |

FIG. 5. Impeller and stage efficiencies for various flow rate coefficients.

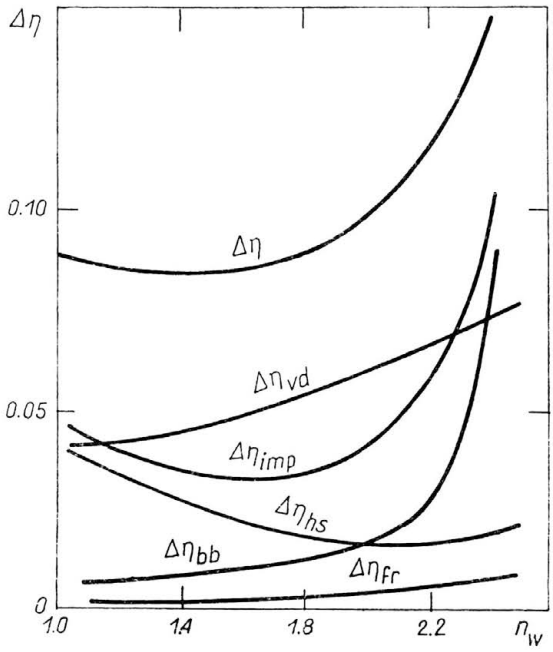


FIG. 6. Stage loss components, $\Phi_0 = 0.1$, $0.03 \leqslant \bar{b}_2 = b_2/D_2 \leqslant 0.06$.

of low $n_w$. Right branches of the curves for $n_w > n_{w\,opt}$ are similar to the calculated data. They show the efficiency decreasing with the increase of $n_w$ due to rising impeller breaking losses.

The centrifugal compressor stage loss as a function of velocity ratio $n_w$ is presented in the Fig. 6. The stage consists of a mixed-flow impeller with outlet blade angle $\beta_2 = 60°$ and vaneless diffusor. The boundary layer friction loss component is a slowly increasing function. When $n_w > 1.8$ the profile losses increase by flow separation on the blade suction side. The hub-to-shroud losses reaches a minimum when $n_w \approx 2.0$. At low values of $n_w$, the non-uniform turbulent core velocity field predominantly influences the growth of hub-to-shroud losses; likewise, the hub and shroud surface losses prevail at high $n_w$ values.

The sum of impeller losses reaches a minimum at $n_w \approx 1.6$. The vaneless diffusor losses increase with $n_w$ since the absolute flow angles are reduced with increasing $n_w$. Therefore the total stage losses $\Delta\eta$ reach a minimum at lower $n_w$ values than the optimal impeller ones. Thus, it is advisable to use optimal velocity ratio interval as $n_w = 1.2...1.4$. It is possible that a three-dimensional analysis would yield more accurate results.

## References

1. Г. Ю. Степанов, *Гидродинамика решеток турбомашин*, с. 463, Физматгиз, Москва 1960.
2. К. П. Селезнев, Ю. Б. Галеркин, *Центробежные компрессоры*, с. 271, Машиностроение, Ленинград 1982.
3. S. V. Patankar, *Numerical prediction of three-dimensional flows Studies in convection; theory, measurement and applications*, v. 1, pp. 1–79, Acad. Press, New York 1975.
4. С. В. Патанкар, Д. Б. Сполдинг, *Тепло-и массообмен в пограничных слоях*, с. 127, Энергия, Москва 1971.
5. В. М. Пасконов, В. И. Полежаев, Л. А. Чудов, *Численное моделирование процессов тепло- и массообмена*, с. 288, Наука, Москва 1984.
6. Л. Г. Лойцянский, *Механика жидкости и газа*, Наука, с. 736, 1978.
7. Ю. В. Лапин, *Турбулентный пограничный слой в сверхзвуковых потоках газа*, 312, Наука, Москва 1983.
8. С. Н. Шкарбуль, *Расчет пространственного пограничного слоя во вращающихся каналах центробежных колес*, № 1, с. 19–21, Энергомашиностроение, 1973.
9. Ю. В. Лапин, М. Х. Стрелец, *Модификация гипотезы Клаузера для равновесных и неравновесных пограничных слоев*, № 3, с. 522–529, Теплофизика высоких температур, 1985.

LENINGRAD POLYTECHNIC INSTITUTE,
LENINGRAD, USSR.

*Received August* 16, 1988.